www.czasopisma.pan.pl PAN www.journals.pan.pl
POLSKA AKADEMIA NAUK

A R C H I V E S O F M E T A L L U R G Y A N D M A T E R I A L S

Volume 59 2014 Issue 3

DOI: 10.2478/amm-2014-0212

W. WOŁCZYŃSKI*, Z. POGODA**, G. GARZEŁ*, B. KUCHARSKA***, A. SYPIEŃ*, T. OKANE****

PART I. THERMODYNAMIC AND KINETIC ASPECTS OF THE HOT DIP (Zn) - COATING FORMATION

CZĘŚĆ I. TERMODYNAMICZNE I KINETYCZNE ASPEKTY FORMOWANIA POWŁOKI CYNKOWEJ METODĄ ZANURZENIOWĄ

A hot dip (Zn) – coating formation is carried out in the industry conditions. Two types of the steel substrate are applied to the experiment. Two morphologically different coatings are obtained, accordingly. A hot dip (Zn) – coating formation is also carried out in the laboratory conditions for making some additional explanations of the revealed phenomena. The thickening of the Γ – phase sub-layer is observed in details to determine time of the transition from stable into meta-stable solidification. The Fe-Zn phase diagrams for stable and meta-stable equilibrium are calculated, respectively. The phase diagram for dissolution is also determined. The criterion of the higher temperature of the solid/liquid (s/l) interface is successfully applied to the Fe-Zn system to justify the competition between stable and meta-stable solidification. The mass balance verification is performed for the (Zn) – coating in order to define the nominal Zn – solute concentration required by dissolution and next by solidification. The Zn – solute concentration in the dissolution, super-saturation and saturation zones are determined thermodynamically. The growth kinetics is described for all the sub-layers in the (Zn) – coating.

Keywords: (Zn) – coatings, meta-stable solidification, phase diagrams, mass balance, growth kinetics, peritectic reaction

Przeprowadzono formowanie powłoki cynkowej metodą zanurzeniową w warunkach przemysłowych. W eksperymencie użyto dwu rodzajów podłoży. Stosownie, uzyskano dwa rodzaje powłok zróżnicowanych morfologicznie. Przeprowadzono również formowanie powłoki w warunkach laboratoryjnych celem uzyskania dodatkowych wyjaśnień dla ujawnionych zjawisk. Szczególnie obserwowano pogrubianie podwarstwy fazy Γ celem określenia momentu przejścia od krystalizacji stabilnej do metastabilnej. Stosownie do tego przejścia obliczono diagramy fazowe Fe-Zn zarówno dla równowagi stabilnej jak i metastabilnej. Dodatkowo obliczono diagram fazowy dla zjawiska rozpuszczania. Skutecznie zastosowano kryterium wyższej temperatury frontu krystalizacji w odniesieniu do diagramu fazowego Fe-Zn celem uzasadnienia współzawodnictwa między krystalizacją stabilną a metastabilną. Przeprowadzono obliczenia bilansu masy dla powłoki (Zn) celem określenia nominalnego stężenia cynku wymaganego przez rozpuszczanie a następnie przez krystalizację. Termodynamicznie określono stężenie cynku w strefach rozpuszczania nasycenia i przesycenia. Kinetyka wzrostu została opisana w odniesieniu do wszystkich podwarstw powłoki cynkowej.

1. Introduction

Some models for the hot dip coating formation make attempt to describe the sub-layers formation with respect to the Fe – Zn phase diagram for stable equilibrium, [1-14]. The kinetics law for the coating growth is widely discussed, [6], [10], [14]. Some investigations associated with the substrate / coating reaction are also known, [2], [5], [12]. However, there are not theoretical descriptions which could be able to describe a flux role in the inter-metallic phase sub-layers formation.

Some observations proved that usually the following phases are visible in the coating: Γ_1, (Fe_3Zn); δ, ($FeZn_7$), ζ, ($FeZn_{13}$) and additionally η, (Zn), [6], [14]. The growth of the δ, ($FeZn_7$) – phase can be split into two separate phenomena: a/ the δ_C – compact phase formation and the δ_P – palisade phase appearance, [7], [14]. The phases Γ_1, (Fe_3Zn); δ, ($FeZn_7$), ζ, ($FeZn_{13}$) are the products of sub-layers formation during the coating growth, [14]. The η, (Zn) – phase is deposited due to the wettability phenomenon when the substrate is pulling out from the bath, [14].

The recent investigation of the Fe-Zn phase diagram for stable equilibrium, [15], was dedicated to the hot-dip galvanizing technology. Therefore, the current model is referred to the above thermodynamic data. One peritectic reaction is visible for the formation of the δ – phase in this phase diagram. Thus, it is obvious that the δ_C – compact phase and the δ_P – palisade phase appear as a product of the same reaction (there are not

* INSTITUTE OF METALLURGY AND MATERIALS SCIENCE, POLISH ACADEMY OF SCIENCES, 25 REYMONTA STR., 30-059 KRAKÓW, POLAND
** JAGIELLONIAN UNIVERSITY, FACULTY OF MATHEMATICS AND COMPUTER SCIENCE, 6 ŁOJASIEWICZA STR., 30-348 KRAKÓW, POLAND
*** CZĘSTOCHOWA UNIVERSITY OF TECHNOLOGY, FACULTY OF PRODUCTION ENGINEERING AND MATERIALS TECHNOLOGY, 19 ARMII KRAJOWEJ STR., 42-200 CZĘSTOCHOWA, POLAND
**** AIST – NATIONAL INSTITUTE OF ADVANCED INDUSTRIAL SCIENCE & TECHNOLOGY, 305 8568 TSUKUBA, UMEZONO 1-1-1, JAPAN

two independent peritectic reactions for the δ_C, δ_P – phases creation as it is suggested in Ref. [18]).

The coating formation requires the application of the $ZnCl_2/NH_4Cl$ – flux. Usually, the flux is immediately transformed into its gaseous form and ash. The chlorine is dominant element in the investigated system. In the first approximation, the Fe-Zn-F ($F = Cl + N + H$) pseudo-ternary system can be treated as the system according to which the sub-layers formation occurs.

The thermodynamic description of the sub-layers formation with the presence of flux is the subject of the current model. This thermodynamic description is referred to the kinetics laws determined for the growth of all phases which appear in the coating due to solidification. The peritectic reactions are also included into the current description.

2. Experiment of the hot-dip coating formation

Some experiments of the hot-dip galvanizing were carried out in the industry conditions (CYNKOWNIA ŚLĄSK, Częstochowa – Poland) for different periods of time. The experiments were performed with the use of two steel substrates, Fig. 1. Finally, the deposition of coatings was completed after 300 [s] of solidification for the first substrate and after 120 [s] for the second substrate.

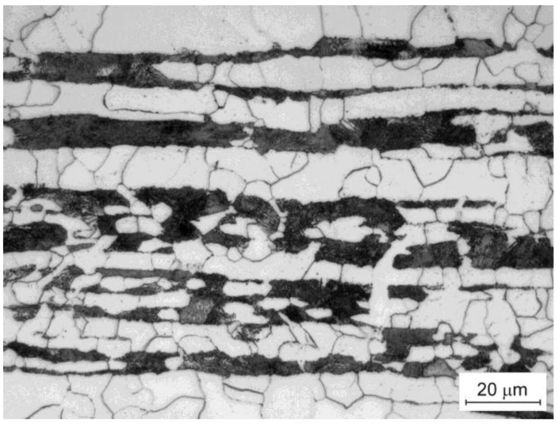

a

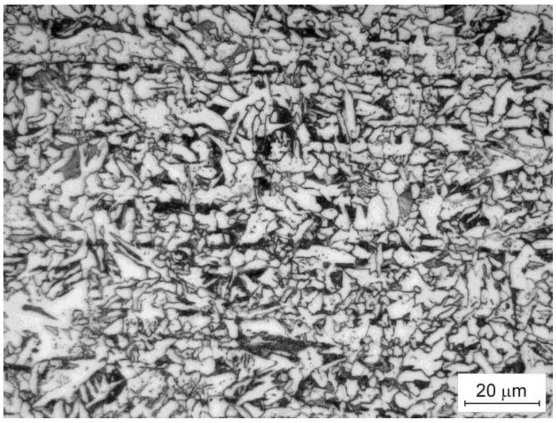

b

Fig. 1. Morphology of the steel substrates used in the experiments, a/the S235 – steel (Fe-0.17C-1.4Mn-0.55Cu); b/the S355 – steel (Fe-0.22C-1.6Mn-0.55Cu-0.55Si); bright areas – *ferrite*, dark areas – *pearlite*

Since the chemical compositions of the steels were different the coating formation followed different kinetics, respectively. The morphology of the both obtained coatings is shown in Fig. 2.

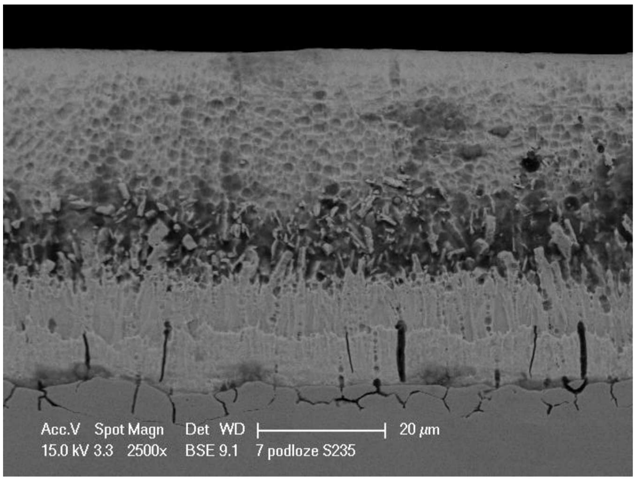

a

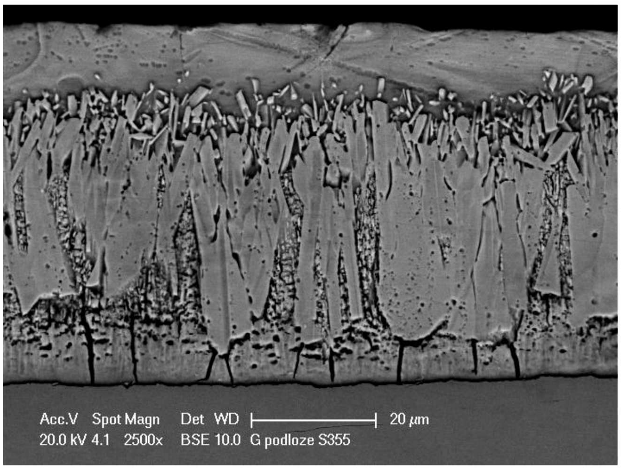

b

Fig. 2. Zinc coatings obtained due to experiments carried out in the industry conditions; a/ the (Zn) – coating on the S235 steel substrate (after 100 [s] of solidification); b/ the (Zn) – coating on the S355 steel substrate (after 60 [s] of solidification)

The creation of the phase sequence, $\Gamma_1/\delta_C/\delta_P/\zeta$, expected in the coating, first has been confirmed by the experiment during which the diffusion joint Fe/(Zn)/Fe was formed in the laboratory conditions, Fig. 3, ($(Zn) \equiv \Gamma_1/\delta_C/\delta_P/\zeta$). The η – phase did not appear in the joint morphology since the liquid filler metal (zinc) had been completely consumed during solidification.

Usually, the ζ – sub-layer consists of two parts: a/ the ζ – columnar phase sub-layer, and b/ the ζ_Z – comb-shaped phase sub-layer. The ζ_Z – sub-layer did not form in the studied joint, Fig. 3.

The thickness of the observed sub-layers was measured with respect to time applied to coatings deposition on both steel substrates, Table 1, Table 2.

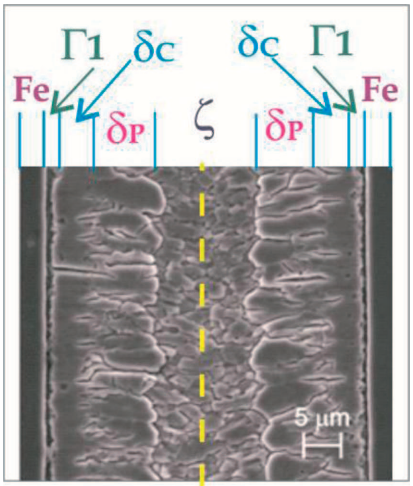

Fig. 3. The phases sequence $Fe/\Gamma_1/\delta_C/\delta_P/\zeta/\delta_P/\delta_C/\Gamma_1/Fe$ in the Fe/(Zn)/Fe diffusion joint (half the joint, till the yellow dashed line, corresponds well to the zinc coating); solidification occurred in the presence of the $ZnCl_2/NH_4Cl$ – flux; the Fe – *armco* was used as a substrate

TABLE 1

Thickness of the phase sub-layers for the S235 steel substrate as measured; birth time of a given phase corresponds with its sub-layer width equal to **0.0** [μm]

time, s	$\Delta\Gamma_1$, μm	$\Delta\delta_C$, μm	$\Delta\delta_P$, μm	$\Delta\zeta$, μm	$\Delta\zeta_Z$, μm
0	**0.0**				
3		**0.0**	**0.0**		
10	1.2	0.8	1.6		
14				**0.0**	**0.0**
20	1.9	3.0	3.0	2.4	4.0
30	2.2	4.0	4.5	3.2	4.6
40	1.9	5.6	5.2	3.9	4.4
60	2.0	7.2	6.8	5.8	4.8
80	2.0	8.4	8.0	6.8	4.5
100	2.0	**9.6**	9.5	7.8	4.7
120	2.0	9.6	10.0	8.5	4.6
140	2.0	9.6	10.6	9.6	4.5
160	2.0	9.6	11.4	10.3	4.7

TABLE 2

Thickness of the phase sub-layers for the S355 steel substrate as measured; birth time of a given phase corresponds with its sub-layer width equal to **0.0** [μm]

time, s	$\Delta\Gamma_1$, μm	$\Delta\delta_C$, μm	$\Delta\delta_P$, μm	$\Delta\zeta$, μm	$\Delta\zeta_Z$, μm
0	**0.0**				
3		**0.0**	**0.0**		
10	0.4	1.7	3.0	**0.0**	**0.0**
20	**0.7**	2.9	4.8	2.8	2.0
30	0.5	5.3	12.6	4.2	3.2
40	0.55	6.2	14.6	5.4	4.0
60	0.6	**7.4**	**18.8**	**6.0**	**5.0**
80	0.6	7.4	28.0	5.0	4.8
100	0.6	7.4	35.4	4.8	5.1

The measurement results of the sub-layers thickness, Table 1, allow for presenting the phase sub-layers thickening in respect to time. At first, the thickening of the Γ_1 – phase sub-layer is subjected to detailed analysis, Fig. 4.

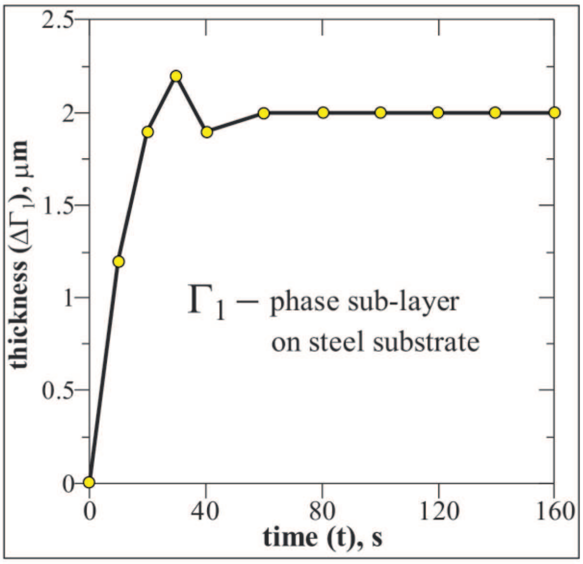

a

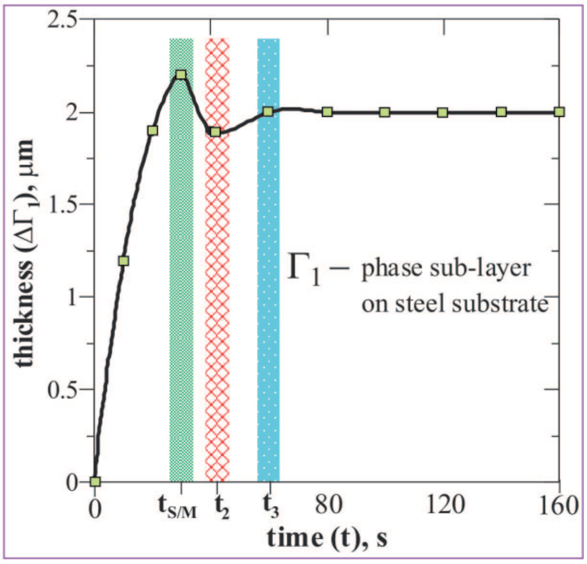

b

Fig. 4. The Γ_1-phase sub-layer thickening; a/ the Γ_1- phase thickening as observed, b/ selected ranges of the thickening: $0 \div t_{S/M}$; $t_{S/M} \div t_2$; $t_2 \div t_3$; $t > t_3$

The stable growth of the Γ- phase occurs for the $0 < t < t_{S/M}$ – time. At the $t_{S/M}$ – time the stable solidification transforms into the meta-stable solidification and therefore the Γ – phase is no more formed, Fig. 4b, Table 1. Next, the solidification follows the phase diagram for the meta-stable equilibrium beginning at the $t_{S/M}$ – time. A precipitation of the δ – phase from the Γ – phase appears within the $t_{S/M} \div t_2$ – period of time. The phenomenon is completed at the t_2 – time, Fig. 4b. The reactions: $\Gamma + \delta \rightarrow \Gamma_1$ and $\delta \rightarrow \Gamma_1$ occur within the $t_2 \div t_3$ period of time. Eventually, the Γ_1 – phase is the stable form after the t_3 – time, Fig. 4b. All the described transformations are explained in Fig. 5. Additionally, the Zn – solute concentration in the Γ_1 – phase is confirmed by the EDS measurements, Fig. 6.

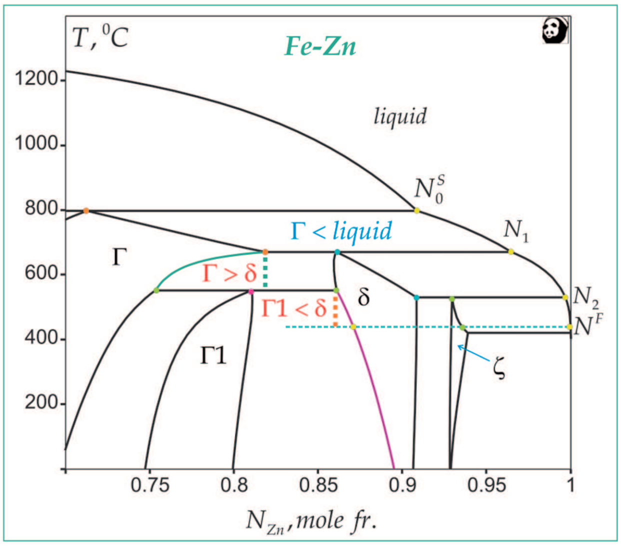

Fig. 5. $\Gamma \rightarrow \Gamma_1$ transformations, as they correspond to the Γ – phase sub-layer thickening / thinning reported in Fig. 4

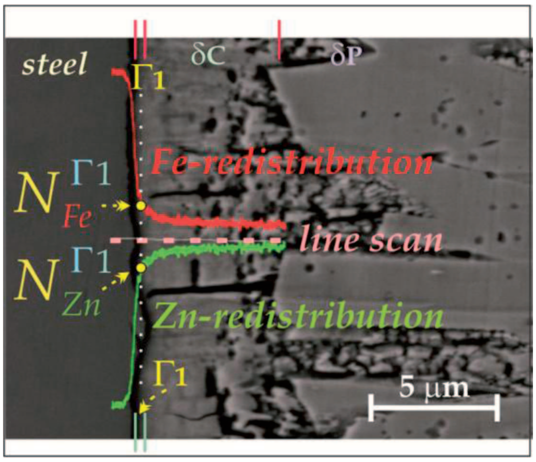

Fig. 6. Zn and Fe redistributions in the Γ_1 – phase sub-layer, $N_{Zn}^{\Gamma 1}$, $N_{Fe}^{\Gamma 1}$ (EDS – technique, S355 steel substrate); additionally, Zn and Fe redistributions in the δ_C phase sub-layer

3. Application of the Fe-Zn phase diagram

The Fe-Zn phase diagram for stable equilibrium is applicable for the period of time, $0 \div t_{S/M}$, when the stable solidification occurs. The Fe-Zn phase diagram has been calculated by means of the ***Pandat Software***, using the data delivered in Ref. [15], Fig. 7. It is assumed that the sub-layers formed during $0 \div t_{S/M}$ – period of time have the average Zn – solute concentration equal to N_0^S, Fig. 7. It was confirmed by the mass balance measurement (average Zn – concentration) in the coating and gave the result: $N_0^S \approx 0.91\, at.\%\, Zn$. The phases solidification is accompanied by the peritectic reactions. However, the reactions are undercooled to the $T_R \approx 450°C$, Fig. 7. The concept of the undercooled peritectic reaction has already been developed, [16], and is adapted to the current model associated with the hot-dip galvanizing technology which occurs at the real temperature, $T_R \approx 450°C$.

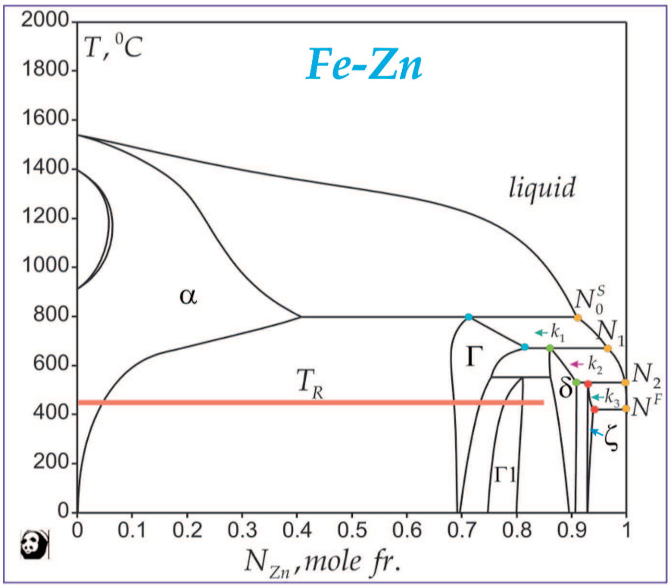

Fig. 7. The Fe-Zn phase diagram for stable equilibrium as calculated due to the data delivered in Ref. [15], (***Pandat Software***)

The undercooled peritectic reactions which appear during the period of stable solidification are : $liquid\,(N_1) + \Gamma \rightarrow \delta$ and $liquid\,(N_2) + \delta \rightarrow \zeta$, Fig. 7. The primary Γ – phase appears due to the solidification path $N_0^S \div N_1$, Fig. 7, and is not completely consumed during the peritectic reaction. Thus, the Γ – phase sub-layer growth is observed during the stable formation of phases for about 30 seconds, Table 1, Fig. 4.

Since the solidification occurs at the constant temperature, $T_R \approx 450°C$, the Number of the Degrees of Freedom should be equal to zero, according to the Gibbs Phase Rule $f = c - p + 1 = 0$. Indeed, $f = 0$, since, $c = 3 \equiv Fe, Zn, F$; $p = 4 \equiv liquid\left(N_0^S\right), \Gamma, \delta, \zeta$. Liquid $N_0^S \approx 0.91\, at.\%\, Zn$ is formed just under the surface of the steel substrate due to the dissolution phenomenon and the phases Γ, δ, ζ are the products of the stable solidification accompanied by the undercooled peritectic reactions, as mentioned.

N^F – means the Zn – solute concentration at the end of solidification path and also the Zn – solute concentration in the bath surrounding the steel substrate. The N^F – definition has already been explained in details for the Ni/Al/Ni joint formation, [17], and applied to the description of the dissolution phenomenon which precedes a solidification of some phases in the mentioned joint, [20]. The N^F – concentration is determined for the Fe-Zn system in Fig. 8. The N^F – concentration is the equilibrium zinc concentration, Fig. 8.

The equilibrium solution, N^F, is the product of the following reaction $remaining\ liquid\,(N_2) + liquid\,(Zn) \rightarrow N^F$, which occurs between third and fourteenth second (within the time period $t_B^\delta < t < t_B^\zeta$), Table 1. At that time, $f = 0$, since, $c = 3 \equiv Fe, Zn, F$ and $p = liquid\left(N_0^S\right), N^F, \Gamma, \delta$. Thus, the Gibbs Phase Rule is also satisfied when the N^F – equilibrium solute solution is forming.

The $t_B^\delta = 3$ – parameter is the time of the δ – phase birth (nucleation), and the $t_B^\zeta = 14$ – parameter is the time of the ζ – phase birth, Table 1.

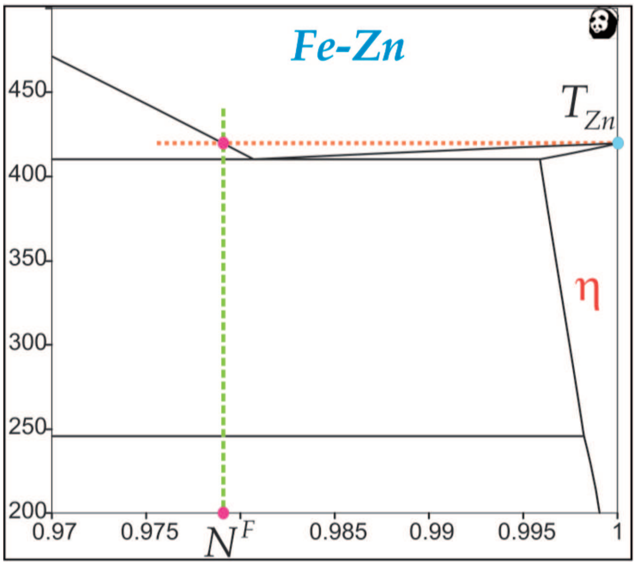

Fig. 8. Determination of the N^F – equilibrium concentration of the zinc for the hot-dip galvanizing technology (a part of the Fe-Zn phase diagram as calculated due to the data delivered in Ref. [15])

The stable period of solidification is transformed into meta-stable solidification at the $t_{S/M}$ – time, Fig. 4. At this time the Γ – phase appearance is no more observed, Table 1, and solidification should be referred to the phase diagram for meta-stable equilibrium. The phase diagram for meta-stable equilibrium calculated by means of the ***Pandat Software*** is shown in Fig. 9.

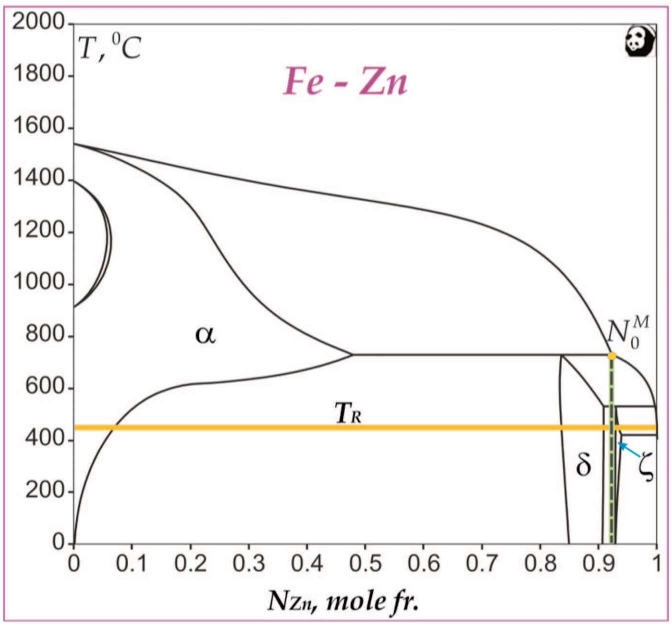

Fig. 9. Fe-Zn phase diagram for meta-stable equilibrium as calculated due to the data delivered in Ref. [15], (***Pandat Software***)

The $N_0^S \rightarrow N_0^M$ – transition occurs at the – $t_{S/M}$ time, with$N_0^M \approx 0.925\,at.\%$, Fig. 9, whereas, $N_0^S \approx 0.91\,at.\%$, Fig. 7.

The $N_0^S \approx 0.91\,at.\%$ solute concentration is the nominal zinc concentration as required by the stable solidification of coating phases. The $N_0^M \approx 0.925\,at.\%$ solute concentration (determined by the mass balance measurement) is the nominal zinc concentration as required by the meta-stable solidification of coating phases.

The solidification is simplified during the meta-stable solidification. The δ – phase formation does not required the occurrence of the peritectic reaction and appears directly due to the *liquidus* →*solidus* partitioning, Fig. 9. The partitioning promotes the creation of the zinc concentration gradient. Thus, the diffusion into the solid forms at the same time, as explained in Ref. [19].

On the other side, the ζ – phase is the product of the peritectic reaction and phenomenon of partitioning accompanied by the diffusion into the solid. The solidification path is shorter than that for the stable solidification $N_0^F(x) \rightarrow N_0^S \rightarrow N^F$ and is now equal to $N_0^F(x) \rightarrow N_0^M \rightarrow N^F$.

Additionally, the Γ – phase formation disappeared, as explained, Fig. 4. As the Gibbs Phase Rule requires $f = 0$ for isothermal solidification it is justified to calculate the Number of the Degrees of Freedom, f. Since the number of elements is $c = 3 \equiv Fe, Zn, F$, thus, p should be equal to 4. Indeed, $p = 4 \equiv liquid\left(N_0^M\right), N^F, \delta, \zeta$ and eventually, $f = 0$.

The $N_0^F(x)$ is the traveling nominal zinc concentration which yields from the Fe-Zn-F – pseudo-ternary phase diagram. This concentration decreases in time since the F – flux disappears when the hot dip galvanizing is in a progress, ($N_0^F(x) \rightarrow N_0^S$, or $N_0^F(x) \rightarrow N_0^M$, respectively).

A part of the ζ – phase cells separates from the ζ_Z sub-layer and flows into the Zn- bath. It is also supposed that the excess Fe – atoms can form the ζ – phase grains within the bath. The presence of the flux particles (ash and chlorine bubbles) promotes the ζ – phase grains appearance.

The experiment with the Fe/(Zn)/Fe joint formation, [22], shows the ζ – phase grains formation in the zinc bath, (especially at the joint centerline), Fig. 10.

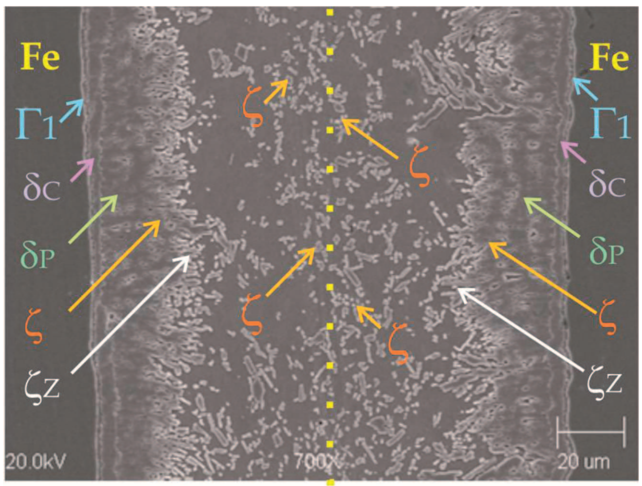

Fig. 10. Fe/(Zn)/Fe – joint as frozen due to the solidification arresting, [22]

Some of the ζ – phase grains become so heavy that they settle down on the bottom to form a zinc silt.

The substitution of the N_0^S – solute concentration, Fig. 7, by the N_0^M – solute concentration, Fig. 9, is the result of the transition from the stable into meta-stable solidification. Additionally, the N_1 – point, Fig. 7, is no more visible in Fig. 9. Moreover, the N_2 – point, Fig. 7, is substituted by the N_2^M – point in Fig. 9. Finally, the δ – phase field is also modified, $\delta_S \rightarrow \delta_M$; δ_S is referred to the phase diagram of the stable equilibrium, Fig. 7; δ_M is referred to the phase diagram for meta-stable equilibrium, Fig. 9.

A part of the δ – phase is engaged into the undercooled peritectic reaction: $k_2 N_2^M + liquid\left(N_2^M\right) \rightarrow k_3 N_2^M$, to form the ζ – phase. A remaining part of the formed ζ – phase is the result of the partitioning along the solidification path, $N_2^M \rightarrow N^F$.

Solidification is always preceded by the substrate dissolution, through the dissolution path, $N^F \rightarrow N_0^M$. The dissolution occurs in the d – dissolution zone. The zinc concentration in the zone is equal to N_0^M, as required by the solidification. As the solute concentration is equal to N_0^M in the d – zone, it is obvious that the average zinc concentration (as measured) across the solidified coating must be equal to the N_0^M, in order to satisfy the mass balance in the considered system.

4. Kinetics of the sub-layers formation in the (Zn) – coating

The measurements of the sub-layers thickness, Table 1, allow for showing phases growth with respect to time, Fig. 11-17.

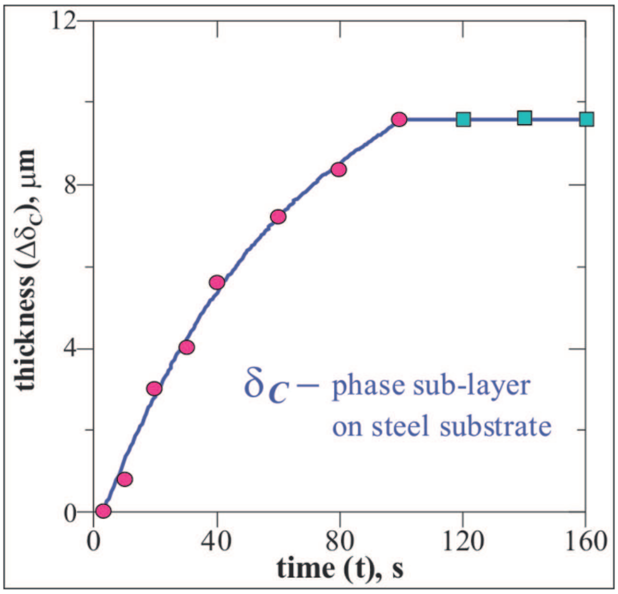

Fig. 11. Tendencies of the δ_C – phase sub-layer thickening within the (Zn) – coating as deposited on the S235 steel substrate (red points and blue points)

Surprisingly, the thickening of the δ_C – phase sub-layer vanished, Table 1. So, this phenomenon will be explained by the current model. First, the thickening of the δ_P – phase sub-layer is the subject of an analysis, Fig. 12.

The behavior of both sub-layers thickening allows for determining the t_0 – time at which the δ_C – phase sub-layer completion is observed, Fig. 13.

The t_0 – time is equal to about 100 seconds, Fig. 13, Table 1. It means that the δ- phase follows two modes of growth. When δ – phase appears as the δ_C – phase it has another morphology than that revealed for the δ_P – phase. It is postulated that the s/l interface of the δ_C – phase is modified by the products of the flux disintegration into gaseous form (chlorine bubbles) and possible transformation into ash/slag.

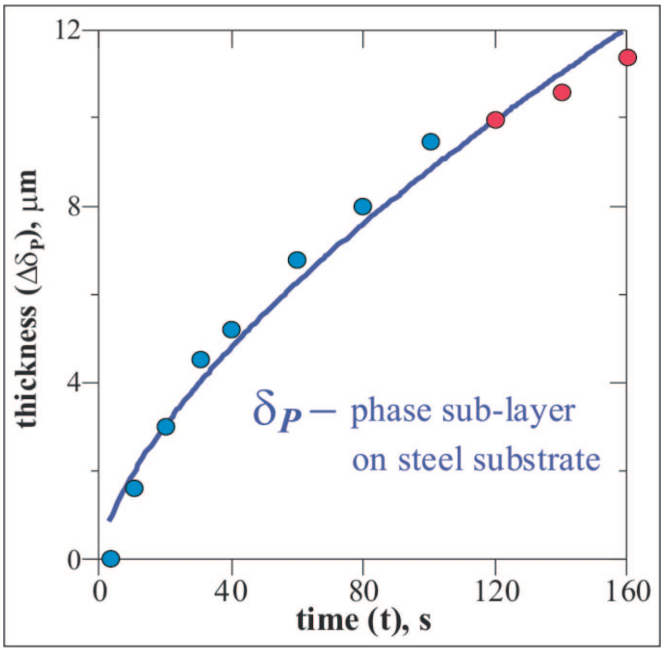

Fig. 12. Tendencies of the δ_P – phase sub-layer thickening in the (Zn) – coating as deposited on the S235 steel substrate (blue points and red points)

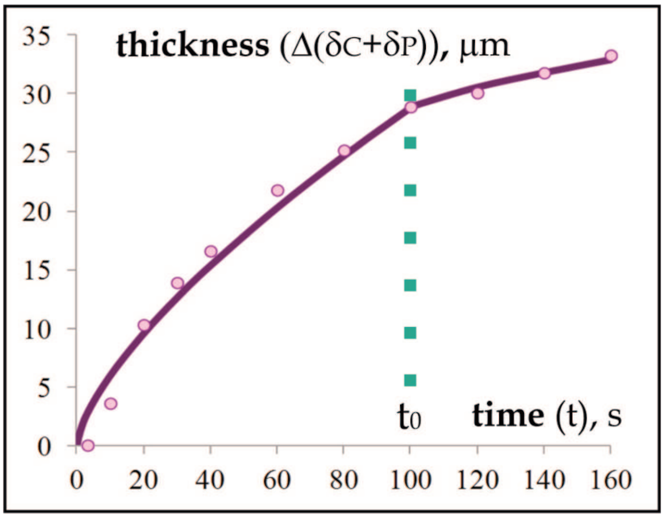

Fig. 13. Kinetics of the $(\delta_C + \delta_P)$ – phases double-layer growth in the (Zn) – coating as deposited on the S235 steel substrate

The products are pushed by the s/l interface and therefore are in the contact with the growing δ_C – phase sub-layer. In the consequence, the specific surface free energy of the δ_C – phase is changed and subsequently the morphology of this phase is different to that presented by the δ_P – phase sub-layer. On the other side, the δ_P – phase sub-layer is formed in the local contact with the pure (Zn) – bath which does not contain the gaseous bubbles and ash/slag. In some situations, the ash/slag layer pushed by the δ_C – phase interface is arrested at the δ_C/δ_P interface and can be revealed in the coating morphology. The arresting is justified because the growth of the δ_C and δ_P – phases occurs at the same time. However, it should be emphasized that the birth of Γ, δ and ζ – phases occurs in sequence, as it has been already discussed on the example of the Ni/Al/Ni diffusion joint formation, [17].

It is obvious that both analyzed phases, δ_C and δ_P, are the product of the same undercooled peritectic reaction as visible in the phase diagram, Fig. 7, (when $t \leqslant t_{S/M}$). The mentioned phases are the product of the solute partitioning as visible in the phase diagram, Fig. 9, (when $t > t_{S/M}$). Thus, there is no need to apply the Fe-Zn phase diagram in which two peritectic reactions are shown, (first, for the δ_{1K}– phase, second, for the δ_{1P}– phase formation, as it was assumed in Ref. [7] and Ref. [18]).

The ζ – phase sub-layer thickening is shown in Fig. 14.

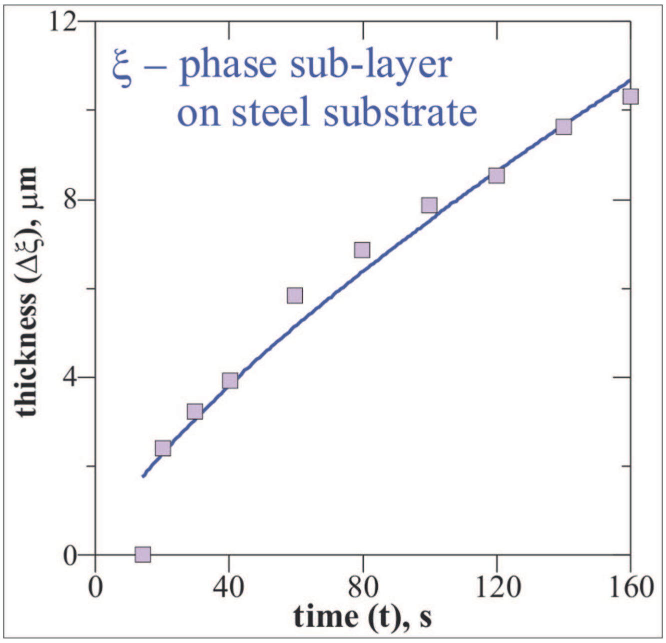

Fig. 14. Tendency of the ζ – phase sub-layer thickening in the (Zn) – coating as deposited on the S235 steel substrate

The kinetics of the $\zeta_Z = \zeta + \eta$ – phases sub-layer is presented in Fig. 15.

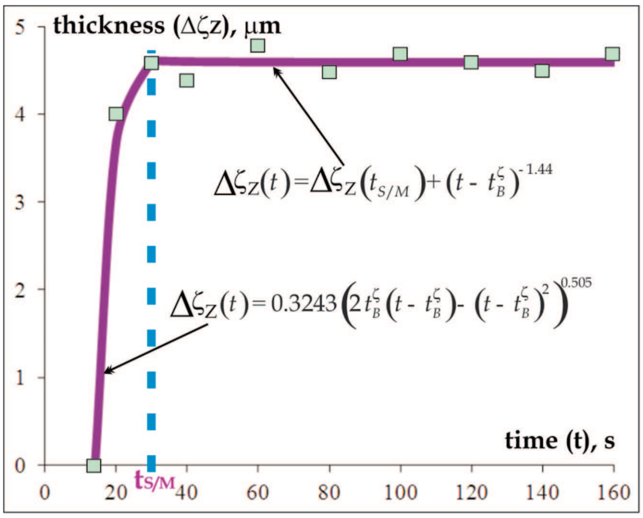

Fig. 15. Kinetics of the ζ_Z – sub-layer growth in the (Zn) – coating as deposited on the S235 steel substrate

The ζ_Z – sub-layer is intensively formed till the $t_{S/M}$ – time, Fig. 15. Beginning from the $t_{S/M}$ – time the ζ_Z – sub-layer growth oscillates between thickening and narrowing. It seems that the optimal thickness of the ζ_Z – sub-layer is conserved in the coating for a given condition of the hot dip galvanizing. Some of the ζ – phase cells are broken off (separated) from the ζ_Z – sub-layer and flow all the time into the zinc bath as illustrated in Fig. 10. They become so heavy that settle down on the bottom to form a zinc silt. However, another ζ – phase cells appear within the ζ_Z – sub-layer for time, $t > t_{S/M}$, Fig. 15. Therefore, the sub-layer conserves its thickness, when $t > t_{S/M}$, Fig. 15.

The common thickening of the sub-layers not perturbed by the tearing, and which results purely from solidification is shown in Fig. 16 and Fig. 17.

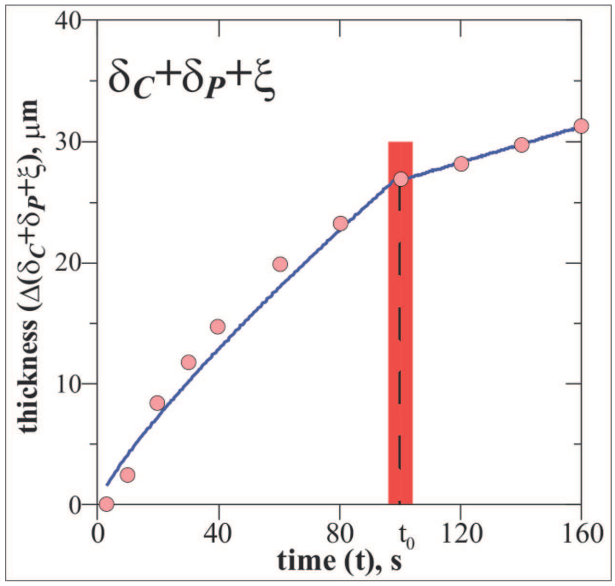

Fig. 16. Tendency of the δ_C, δ_P and ζ – phase sub-layers thickening in the (Zn) – coating as deposited on the S235 steel substrate

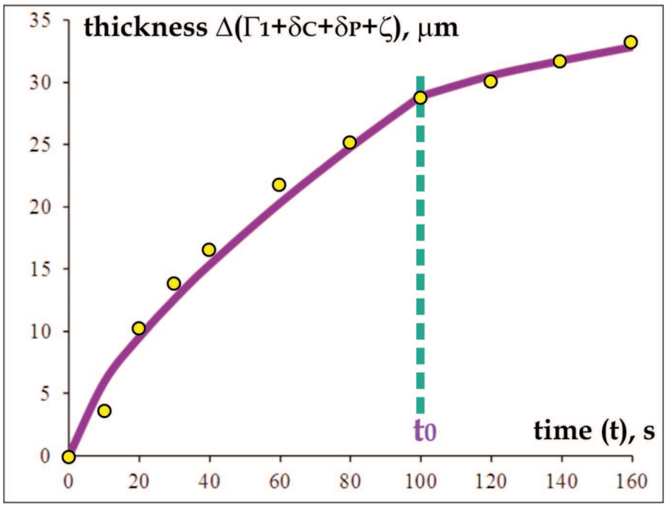

Fig. 17. Kinetics of the Γ_1, δ_C, δ_P and ζ – phase sub-layers growth in the (Zn) – coating as deposited on the S235 steel substrate

5. Competition between stable and meta-stable solidification

Some periods of stable or meta-stable solidification appear during the zinc coating formation, [23]. The experiment, Table 1, Table 2 and analysis of the Γ – phase formation,

Fig. 4, allow for determining the $t_{S/M}$ – time at which the meta-stable solidification becomes a winner in the competition between both processes. Consequentially, two phase diagrams have been applied in the description of the coating formation, Fig. 7, Fig. 9, respectively.

Moreover, the solidification is always accompanied by a dissolution, [21]. The d – dissolution zone can be distinguished within the substrate, [22]. In the (Zn) – coating formation, the zone is formed due to the Zn – solute diffusion into the steel as long as the d – zone becomes liquid. Next, a diffusion of the liquid from the zone towards the sub-layers front ensures the sub-layers thickening. So, thickening results from solidification of the liquid coming from the zone. Thus, dissolution and solidification are the coupled phenomena. For that reason, the ***Pandat*** Software was applied to calculate the Fe-Zn phase diagram for dissolution, Fig. 18.

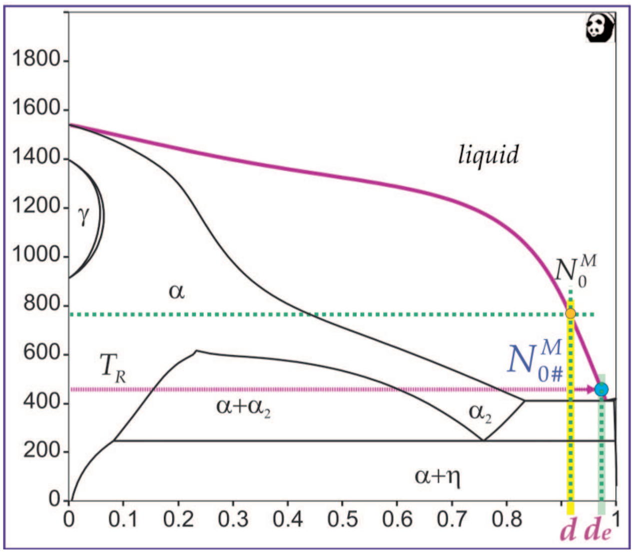

Fig. 18. Fe-Zn phase diagram for dissolution as calculated with the use of the data delivered in Ref. [15]

The average Zn – solute redistribution measured across the coating (across its part which is the product of solidification: $\Gamma 1 + \delta_C + \delta_P + \zeta$ sub-layers) is equal to the N_0^S – concentration for the stable solidification, Fig. 7. The average Zn – solute redistribution measured across the coating (across its part which is the product of solidification: $\delta_C + \delta_P + \zeta$ sub-layers) is equal to the N_0^M – concentration for the meta-stable solidification, Fig. 9. Subsequently, the N_0^M – solute concentration is introduced into the phase diagram for dissolution, Fig. 18. This localization of the N_0^M – concentration in Fig. 18, is justified by the mass balance (the Zn – solute concentration must be the same in the d – dissolution zone as the N_0^M – average solute concentration measured in the solidified part of the coating).

However, the coming up to the N_0^M – solute concentration in the d – zone does not ensure its complete melting at the imposed, T_R – real temperature, Fig. 18. Thus, the reaching of the N_0^M – solute concentration is not sufficient to form the d – zone fully liquid.

At the T_R – real temperature the excess $N_{0\#}^M$ – solute concentration (blue point at the intersection of the T_R – isotherm and *liquidus* line) is to be reached in the d – zone (named now as the d_e - zone), Fig. 18. Thus, the difference, $N_{0\#}^M - -N_0^M$, (excess Fe – atoms in the zinc bath) is responsible for the appearance of the excess ζ – cells in the ζ_Z – sub-layer and first of all for the nucleation of the excess ζ – grains which flow in the bath, Fig. 10. The solidification of the excess ζ – phase ensures the mass balance in the d_e – zone / coating / surrounding bath system, under condition that the $N_{0\#}^M < N^F$ – inequality is satisfied.

The arrow shows precisely the localization of the d_e – dissolution zone in the phase diagram with the $N_{0\#}^M$ – solute concentration, Fig. 18. Thus, the N_0^S and next N_0^M – solute concentrations in the dissolution zone are adequate for the $\Gamma 1 + \delta_C + \delta_P + \zeta$ – basal sub-layers formation, only.

The above discussed mass balance is not yet satisfied within the period of time when a given phase is just born. The good example of this situation is recorded in Fig. 19, where the ζ – phase birth is visible. Some small nuclei appear before the ζ – phase sub-layer is formed in full.

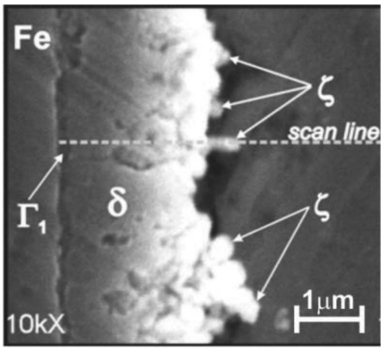

Fig. 19. Nucleation (birth) of the ζ – phase on the surface of the δ – phase sub-layer, at time t_B^ζ; the (Fe) – *armco* substrate was applied in the experiment and solidification occurred without the presence of a flux; thus, one phase, δ, appeared in the coating, only, [22]

The calculated phase diagram for dissolution (from Fig. 18), is superposed over the phase diagram for meta-stable solidification (from Fig. 9), to show coincidence of both diagrams and some characteristic points, Fig. 20.

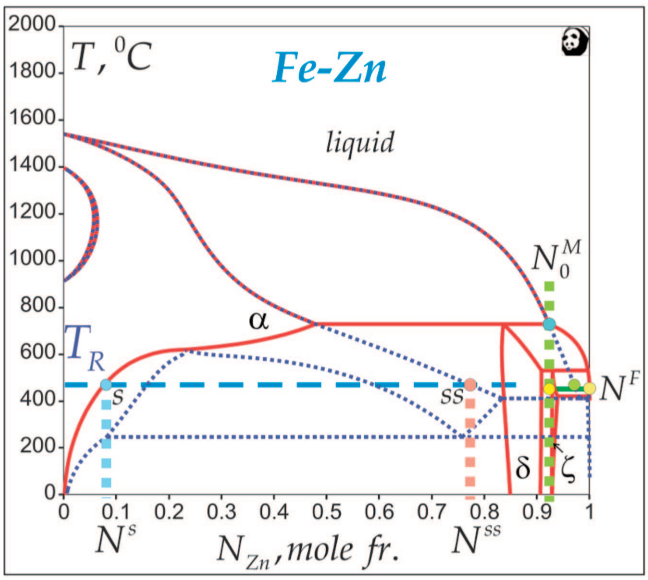

Fig. 20. Superposition of the phase diagrams for meta-stable solidification and dissolution

The T_R – real temperature (blue dashed line) of hot dip coating formation intersects some equilibrium lines of diagrams. Thus, s – saturation solution with the N^s – solute concentration and ss – supersaturation solution with the N^{ss} – solute concentration are defined. $N^s = 0.08$ and $N^{ss} = 0.77$ [mole fr.]. The bright green point indicates the exces $N_{0\#}^M$ – solute concentration required in the dissolution zone, $N_{0\#}^M < N^F$. Moreover, solidification path, $N_0^M \to N^F$, (along the *liquidus* line) as well as dissolution path, $N^F \to N_0^M$, (dark green line which connects two yellow points) are also indicated. So, the superposition of phase diagrams, Fig. 20, shows how the considered system oscillates between dissolution zone formation and sub-layers thickening.

The d – dissolution zone is also defined in Fig. 20 (the dotted green vertical line). This zone is infinitesimally small and therefore the Zn – solute concentration cannot be measured by the EDS technique. Thus, a suggested localization of the d – dissolution zone is marked on the Zn – redistribution curve, only, Fig. 21.

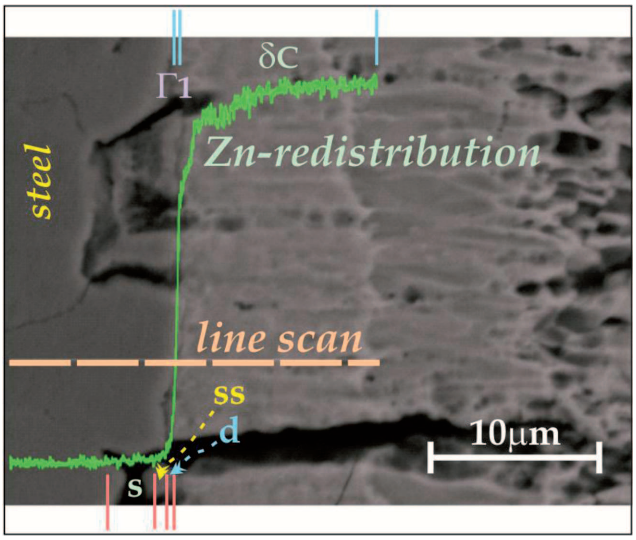

Fig. 21. Zn – solute redistribution in the vicinity of the substrate / coating interface; the postulated localizations of: d – dissolution zone, ss – supersaturation zone and s – saturation zone in the steel substrate

The Zn – solute redistribution (segregation) has been revealed in the substrate, Fig. 21. However, the Zn – solute redsitribution is more significant in the coating, across the δ_C - phase sub-layer, Fig. 21.

Other alloying elements can also segregate, [13]. In the case of the current EDS analysis the significant diffusion of carbon from the steel substrate to the coating and subsequently, its segregation across the δ_C – sub-layer has been revealed.

The Zn – solute redistribution is more intensive during the first period of the δ_C – sub-layer formation, Fig. 21. The first period can be referred to the stable solidification accompanied by the steep redistribution gradient. The second period is associated with the meta-stable solidification which is accompanied by the moderate redistribution gradient, Fig. 21.

Thus, even the existence of two types of the Zn – solute redistribution profiles, Fig. 21, confirms that the transition from stable solidification into meta-stable solidification occurred during the hot dip coating formation.

The meta-stable solidification is the winner in the competition at time, $t_{S/M}$, Fig. 4. This victory can be justified theoretically through the satisfaction of the inequality $T_\delta^* > T_\Gamma^*$, Fig. 22. According to this criterion, the δ – phase formation is the winner in the competition because the δ – phase has a higher temperature of its s/l interface, in comparison with the s/l interface temperature of the Γ – phase, [24].

In the consequence, the δ – phase solidification substitutes the Γ – phase solidification, Fig. 9. It occurs, in spite of the fact that the virtual localization of the N_0^M – parameter on the *liquidus* line, Fig. 7, would suggest the Γ – phase appearance.

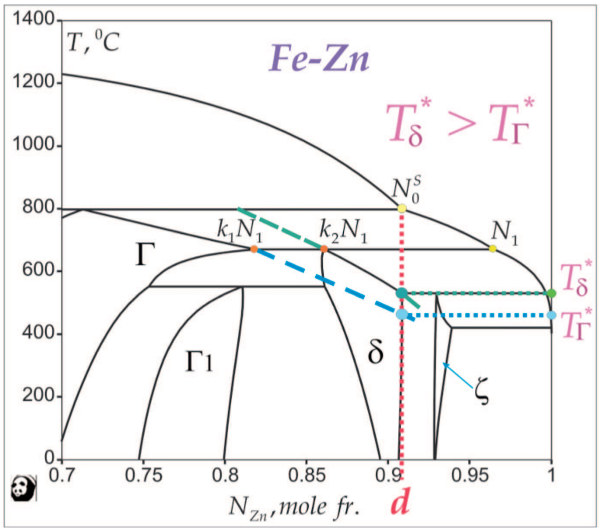

Fig. 22. Application of the criterion of the higher temperature of the s/l interface to the hot dip coating formation; T_Γ^* – temperature of the s/l interface for the Γ – phase solidification; T_δ^* – temperature of the s/l interface for the δ – phase solidification

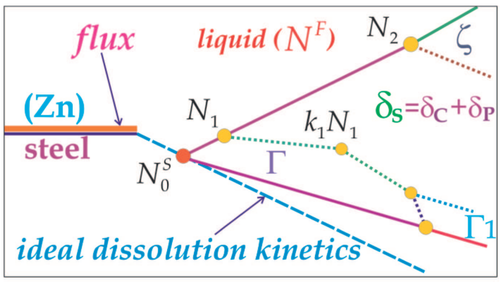

a

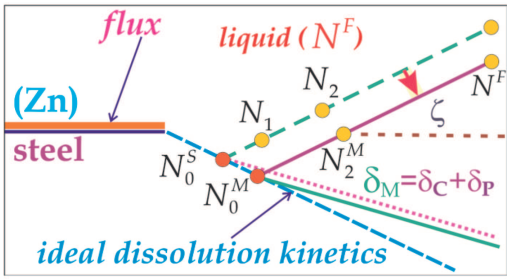

b

Fig. 23. Kinetics of: a) stable, ($t < t_{S/M}$), b) meta-stable solidification ($t_{S/M} < t$)

The intersections of the N_0^S – solute concentration (vertical dotted line) with the *solidus* lines of Γ – phase and δ – phase yield the mentioned inequality, Fig. 22.

The transformation of the stable solidification, Fig. 23a, into the meta-stable solidification, Fig. 23b, results in the $N_0^S \to N_0^M$ – concentration change in the dissolution zone (red arrow in Fig. 23b). Finally, the δ_S – stable phase field, Fig. 23a is replaced by the δ_M – meta-stable phase field, Fig. 23b.

6. Concluding remarks

The phases nucleation in the (Zn) – coating is sequential; the Γ – phase is born at time $t_B^\Gamma = 0$ [s], δ_C,δ_P – phases are visible at time $t_B^\delta = 3$ [s], and the ζ – phase appears at time $t_B^\zeta = 14$ [s], Table 1.

The Gibbs Phase Rule (with the Number of the Degrees of Freedom equal to zero) is satisfied during isothermal solidification of the (Zn) – coating.

The stable solidification (with the Γ – phase formation) is determined by the time $t_{S/M} = 30$ [s], where, the $t_{S/M}$ is the threshold value of time for the stable/meta-stable transition, Fig. 4a.

The transition from the stable solidification to the meta-stable solidification involves the transformation of the δ – phase field in the Fe-Zn phase diagram, $(\delta_S \to \delta_M)$, Fig. 23.

The presence of flux is responsible for the δ_C – phase sub-layer formation. It results from the fact, that the flux is pushed by the δ_C – phase s/l interface during solidification. Therefore, the specific surface free energy of the δ_C – phase is not the same as that of the δ_P – phase. Thus, δ_C – phase differs from δ_P – phase in its morphological appearance.

The solidification is always preceded by the substrate dissolution. The N^F – liquid solution diffuses into the d – dissolution zone as long as the zone reaches the $N_{0\#}^M$ – solute concentration in order to become liquid, Fig. 18.

The N_0^M – solute concentration in the dissolution zone is adequate to satisfy the needs of the meta-stable solidification, $(\delta_C, \delta_P, \zeta$ – phases formation). Therefore, the excess solute concentration in the zone, $N_{0\#}^M - N_0^M$, results in the excess ζ – phase formation (the excess ζ – phase is localized in the ζ_Z – sub-layer and in the bath, Fig. 10).

The N_0^M, $N_{0\#}^M$ – solute concentrations are not localized at some characteristic points on the *liquidus* line, Fig. 18. It could be supposed that localization of both concentrations in the phase diagram is accidental. However, the superposition of phase diagrams for meta-stable equilibrium (associated with dissolution and connected to solidification), Fig. 20, confirms that the localization of the N_0^M – solute concentration is thermodynamically selected. The N_0^M – solute concentration is situated on the tie-line for the beginning of the δ – phase precipitation during the meta-stable solidification. Analogously, the N_0^S – solute concentration is situated on the tie-line for the beginning of the Γ – phase precipitation during the stable solidification, Fig. 7. On the other side, the localization of the $N_{0\#}^M$ – solute concentration depends on the value of the T_R – real temperature applied to the hot dip coating formation.

Not only the phases birth is sequential but they appear also sequentially during solidification, according to their localizations in the phase diagram. Moreover, the thicknesses of the Γ, δ, ζ – phase sub-layers in the coating are proportional to the adequate solidification paths. It has already been confirmed for a similar technology with the use of the Ni -Al system, [25].

Exceptionally, the difference in the thicknesses of the δ_C – phase sub-layer and the δ_P – phase sub-layer is the result of the influence of the products of the flux disintegration on the δ_C – phase sub-layer kinetics.

Generally, the results gathered in Table 1 and Table 2 reveal the influence of two different substrates (influence of their structure and elements content) and the flux on the sub-layers thickening.

In the case of the (Zn) – coating formation on the steel S235 substrate the thicknesses of both δ_C – phase sub-layer and δ_P – phase sub-layer are comparable each to other for the time, $t < t_0$, $t_0 = 100$ [s], Table 1.

However, in the case of the (Zn) – coating formation on the S355 steel substrate the thicknesses of both δ_C – phase sub-layer and δ_P – phase sub-layer differ significantly each from other for the time, $t < t_0$, $t_0 = t_{\zeta\to\delta} = 60$ [s], Table 2. The $t_{\zeta\to\delta}$ is the time of the beginning of the so-called "*mantis*" phenomenon according to which the ζ – phase is progressively consumed by the δ – phase (solid state transformation).

The "*mantis*" phenomenon is defined as: $\zeta\,(FeZn_{13}) \to \delta\,(FeZn_{10}) + liquid\,(3Zn)$. It is postulated that the liquid (Zn) precipitates at the ζ/η boundary.

The Gibbs Phase Rule is also satisfied during the "*mantis*" phenomenon; $f = 0$, because $c = 2 = Fe, Zn$, and $p = 3 = \delta, \zeta, liquid\,(Zn)$, with $T_R = const$.

The steel substrate contains carbon which diffuses into the coating. This phenomenon improves the substrate / coating adhesion. The carbon also changes the specific surface free energy of a given s/l interface. Moreover, the carbon diffusion into the coating has an effect on the kinetics of a given sub-layer growth and on the appearance of the "*mantis*" phenomenon observed at the $t_{\zeta\to\delta}$ – time.

On the other side, the kinetics of the ideal dissolution, Fig. 23, is continuously retarded by the cluttering of the external channels (channels between cells within a given sub-layer) and by the increasing diffusion distances. In the current model ideal substrate dissolution occurs with the use of the external channels (boundary diffusion), only. The ideal thickening is possible due to the bulk diffusion (through the cells), only. In fact, both types of diffusion are exploited for the substrate dissolution or for the sub-layers thickening.

It is assumed in the current model that the index of the power satisfies the following inequality $0.5 \leqslant m \leqslant 1$ in the kinetics law $\Delta p = k_p\, t^m$, with $p = \Gamma, \delta, \zeta$, which describes the growth of the phase sub-layers. Additionally, $m = 1$, when the diffusion occurs through the external channels, and $m = 0.5$, when the bulk diffusion is effective, only.

For example, the thickening of the δ – phase, Fig. 13, follows different kinetics laws: $\Delta\left[\delta_C + \delta_P\right](t) = 1.35\,\left(t - t_B^\delta\right)^{0.58}$, $t \in [0, t_0]$; $\Delta\left[\delta_C + \delta_P\right](t) = \Delta\left[\delta_C + \delta_P\right](t_0) + 0.15\,(t - t_0)^{0.65}$, $t_0 < t \leqslant t_K$, with, $t_0 = 100$ [s], and $t_K = 300$ [s].

So, $m = 0.58$ or $m = 0.65$ for the thickening of the δ – phase sub-layers. It becomes obvious that both boundary diffusion (through the channels) and bulk diffusion (through cells) are employed simultaneously in the sub-layers growth because $m \neq 0.5$.

REFERENCES

[1] A. B o h r a n - T a v a k o l i, Formation and growth of the δ 1 phase in the Fe-Zn system. Part 1. Zeitschrift für Metallkunde **75**, 350-355 (1984).

[2] J. I n a g a k i, M. S a k u r a i, T. W a t a n a b e, Alloying reactions in hot dip galvanizing and galvannealing processes. ISIJ International **35**, 1388-1393 (1995).

[3] C.E. J o r d a n, A.R. M a r d e r, Fe-Zn phases formation in interstitial – free steels hot-dip galvanized at 450°C. Journal of Materials Science **32**, 5593-5602 (1997).

[4] J.D. C u l c a s i, P.R. S e r e, C.I. E l s n e r, A.R. S a r l i, Control of the growth of zinc – iron phases in the hot dip galvanizing process. Surface and Coatings Technology **122**, 682-686 (1999).

[5] E. S c h e i l, H. W u r s t, Über die reaktionen des eisens mit flüssigem zink. Zeitschrift für Metallkunde **29**, 225-228 (1937) (in German).

[6] D. K o p y c i ń s k i, Krystalizacja faz międzymetalicznych i cynku na żelazie oraz na jego nisko- i wysokowęglowych stopach podczas procesu cynkowania, Rozprawy Monografie AGH **149**, 131 (2006) (in Polish).

[7] M.A. G h o n i e m, K. L o h b e r g, Über die feuerverzinkung entstenden δ 1p und δ 1k schichten, Metall **26**, 1026-1030 (1972) (in German).

[8] P.J. G e l l i i n g s, E.W. B r e e, G. G i e r m a n, Synthesis and characterization of homogeneous intermetallic Fe-Zn compounds. Part1. Zeitschrift für Metallkunde **70**, 312-314 (1979).

[9] P.J. G e l l i i n g s, E.W. B r e e, G. G i e r m a n, Synthesis and characterization of homogeneous intermetallic Fe-Zn compounds. Part 2. Zeitschrift für Metallkunde **70**, 315-317 (1979).

[10] C.E. J o r d a n, A.R. M a r d e r, Morphology development in hot-dip galvanneal coatings. Metallurgical and Materials Transactions **25A**, 937-947 (1994).

[11] C.R. X a v i e r, U.R. S e i x a s, P.R. R i o s, Further experimental evidence to support a simple model for iron enrichment in hot-dip galvanneal coatings on IF steel sheets. ISIJ International **36**, 1316-1317 (1996).

[12] M. D a n i e l e w s k i, Diffusion in multicomponent systems, Archives of Metallurgy and Materials **49**, 189-200 (2004).

[13] M. Z a p p o n i, A. Q u i r o g a, T. P e r e z, Segregation of alloying elements during the hot-dip coating solidification process, Surface and Coatings Technology **122**, 18-20 (1999).

[14] J. M a ć k o w i a k, N.R. S h o r t, Metallurgy of galvanized coatings, International Metals Reviews **237**, 1-19 (1979).

[15] W. X i o n g, Y. K o n g, Y. D u b, L. Z i k u i, M. S e l l e b y, S. W e i h u a, Thermodynamic investigation of the galvanizing systems, I: Refinement of the thermodynamic description for the Fe-Zn system, CALPHAD: Computer Coupling of Phase Diagrams and Thermo-Chemistry **33**, 433-440 (2009).

[16] Y.K. C h u a n g, D. R e i n i s c h, K. S c h w e r d t f e g e r, Kinetics of diffusion controlled peritectic reaction during solidification of iron-carbon alloys, Metallurgical Transactions **6A**, 235-238 (1975).

[17] W. W o ł c z y ń s k i, T. O k a n e, C. S e n d e r o w s k i, D. Z a s a d a, B. K a n i a, J. J a n c z a k - R u s c h, Thermodynamic justification for the Ni/Al/Ni joint formation by a diffusion brazing, International Journal of Thermodynamics **14**, 97-105 (2011).

[18] J. S c h r a m m, Über eine neue phase in system eisen – zink, Zeitschrift für Metallkunde **29**, 222-225 (1937) (in German).

[19] W. W o ł c z y ń s k i, Back-diffusion phenomenon during the crystal growth by the Bridgman method, Chapter 2. in the book: Modelling of Transport Phenomena in Crystal Growth, p.19-59, WIT Press, Southampton–Boston), 2000, eds. J. Szmyd & K. Suzuki.

[20] W. W o ł c z y ń s k i, J. J a n c z a k - R u s c h, J. K l o c h, T. R u t t i, T. O k a n e, A model for solidification of intermetallic phases from Ni-Al system and its application to diffusion soldering, Archives of Metallurgy and Materials **50**, 1055-1068 (2005).

[21] I. T u a h - P o k u, M. D o l l a r, T. M a s s a l s k i, A study of transient phase bonding process applied to a Ag/Cu/Ag sandwich joint, Metallurgical Transactions **19A**, 675-686 (1988).

[22] W. W o ł c z y ń s k i, E. G u z i k, D. K o p y c i ń s k i, T. H i m e m i y a, J. J a n c z a k - R u s c h, Mass transport during diffusion soldering or brazing at constant temperature, Proceedings of the 13^{th} International Heat Transfer Conference, Sydney 2006, ed. begell house, inc. publishers, eds G. de Vahl & E. Leonardi, CD, (2006), MST-11, 12 pages.

[23] P. P e r r o t, J.C. T i s s i e r, J.Y. D a u p h i n, Stable and metastable equilibria in the Fe-Zn-Al system at 450°C, Zeitschrift für Metallkunde **83**, 786-790 (1992).

[24] T. U m e d a, T. O k a n e, W. K u r z, Phase selection during solidification of peritectic alloys, Acta Materialia **44**, 4209-4216 (1996).

[25] W. W o ł c z y ń s k i, T. O k a n e, C. S e n d e r o w s k i, B. K a n i a, D. Z a s a d a, J. J a n c z a k - R u s c h, Meta-stable conditions for diffusion brazing, Archives of Metallurgy and Materials **56**, 311-323 (2011).

Received: 20 January 2014.